

RSC Advances



This is an *Accepted Manuscript*, which has been through the Royal Society of Chemistry peer review process and has been accepted for publication.

Accepted Manuscripts are published online shortly after acceptance, before technical editing, formatting and proof reading. Using this free service, authors can make their results available to the community, in citable form, before we publish the edited article. This *Accepted Manuscript* will be replaced by the edited, formatted and paginated article as soon as this is available.

You can find more information about *Accepted Manuscripts* in the [Information for Authors](#).

Please note that technical editing may introduce minor changes to the text and/or graphics, which may alter content. The journal's standard [Terms & Conditions](#) and the [Ethical guidelines](#) still apply. In no event shall the Royal Society of Chemistry be held responsible for any errors or omissions in this *Accepted Manuscript* or any consequences arising from the use of any information it contains.

Superior Relaxation of Stresses and Self-Healing Behavior of Epoxy-Amine Coatings

Maurizio Villani^{*}, *Yogesh S. Deshmukh*¹, *Caghan Camlibel*, *A. Catarina C. Esteves* and *Gijsbertus de With*^{*}

Laboratory of Materials and Interface Chemistry,
Eindhoven University of Technology, Den Dolech 2, P.O. Box 513, 5600 MB
Eindhoven, The Netherlands.

* To whom correspondence should be addressed.

E-mail: M.V.Villani@tue.nl; G.deWith@tue.nl, Phone: +31-40-2473132/+31-40-2474947.

Abstract. Cross-linked epoxy resins are amongst the most widely used materials for protecting metal surfaces in high performance applications. During curing or application of such materials as a coating on a metal surface, mechanical stresses can build up and ultimately lead to mechanical failure. Stress-relaxation in fully covalent systems is, however, limited due to the restricted mobility of the network chain segments. Hereby, we introduce physical cross-links (hydrogen bonds into the epoxy-amine network) via the incorporation of amide motifs, which enhance temporary local network mobility and ensures a better ability to relax the stresses preemptively, without any significant change in modulus and (dry and wet) adhesion behavior. The reversibility of hydrogen bonds also results in superior restoration of superficial scratches with no detrimental effect on the original adhesion properties of the material.

Keywords: Epoxy resins; Coatings; Hydrogen bonding; Adhesion; Preemptive healing.

¹ Present address: Polymer Science and Technology Group, Faculty of Science, Maastricht Science Program, Maastricht University, P.O. Box 616, 6200 MD, Maastricht, the Netherlands.

Introduction

Polymer coatings are essential in our daily lives either to decorate or to protect surfaces from the environment, e.g., from moisture, UV-radiation, chemical attack or mechanical damage [1]. The performance and lifetime of coating materials are strongly dependent not only on the materials intrinsic properties, but also on adhesion between the coating and substrate [2].

Epoxy resins are amongst the most used materials for coating applications due to their excellent stability, i.e., chemical and physical resistance, good adhesive performance, ease of handling and outstanding mechanical and electrical properties [3-5]. Therefore epoxy resins are widely utilized for protecting metal substrates from corrosion and as matrix material for structural composites, in high performance applications such as in aerospace and marine [6, 7]. Besides the type of epoxide and amine, the curing process and the type of curing agent used during polymerization/cross-linking of the epoxy resin determine their final coating properties [8-10].

There is a multitude of factors which may change the mechanical behavior of polymeric coatings on metal substrates. Mechanical stresses may arise during application of a coating due to an increase in density upon cross-linking, or shrinkage upon evaporation of the solvent. Furthermore, the differences in thermal expansion coefficient between the coating and substrate, the deformation of the substrate and the chemical ageing or damaging of the coating can also contribute to the presence of internal stress [11]. All these factors affect the mechanical behavior of coatings, decrease their lifetime and ultimately lead to failure. To solve this problem but still taking advantage of the long-lasting, outstanding properties of epoxy-based coatings, several attempts were made to introduce self-healing mechanisms [12, 13], in order to repair external damages and extend their lifetime further.

The self-healing materials concept aims at the recovery of a lost property/functionality, maintaining a high level of performance throughout an extended service lifetime [14]. In an

ideal self-healing material, multiple healing events can take place, fully restoring the initial material properties and resulting in an infinite “theoretical” service lifetime. However, for most of the current, “real” self-healing systems, the healing event(s) only restore partially the initial properties leading to a slower degradation of the material (as compared to non-healable coatings). An important cause for failure in polymer coatings is crack formation and propagation; therefore, repairing cracks and mitigating the failure mechanism(s) in an early stage may prevent further propagation, thus extending the life span of the materials [15, 16].

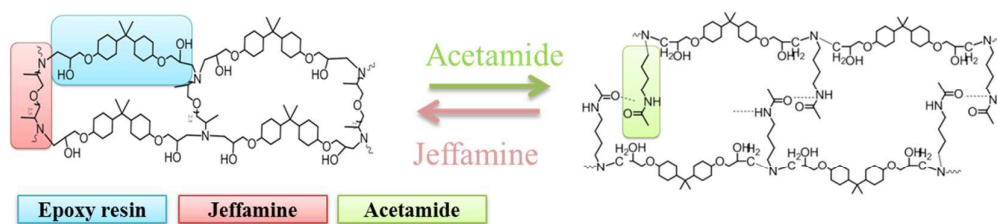
Self-healing of damage can be autonomous (without external triggers) or non-autonomous (i.e., triggered by heat or pressure) [17]. Moreover, self-healing materials can be categorized as extrinsic or intrinsic, based on their “healing” mechanism. For the first category, microcapsules, hollow fibers or microvascular networks are typically embedded in the material matrix to enable self-healing behavior. Upon damage, these added components fracture and release a healing agent filling and eventually sealing the crack, preventing its propagation [18-22]. For the second category, the material is chemically modified to reestablish chemical bonds, after being broken by the damage, i.e., reversible cross-linking.

Intrinsic self-healing usually requires external stimuli such as light, heat or oxygen to trigger the healing process and reestablish the broken chemical bonds. This healing mechanism depends on the matrix polymer architecture and typically consists of two steps. First, a “softening” step enhancing local mobility in the proximity of the damage which requires a decrease in local viscosity, leading to the local and temporary network mobility required for flow and damage repair. Second, after the healing trigger is removed, a “hardening” process leads the restoration of the original local viscosity and recovery of the materials properties [14]. Various types of reversible chemical or physical cross-links have been employed to control the local viscosity with different healing processes and degree of reversibility. Typical examples are provided by the use of Diels-Alder (DA) and Retro-DA

reactions, [21, 23-25] ionomers, [26, 27] thiol-based chemistry [21, 28, 29] and supramolecular polymers [23, 26, 27, 30-34]. An overview of the various options is provided by Michael et al. [33]. The self-healing mechanism based on supramolecular polymers is attributed to the connection/reconnection of non-covalent bonds provided by their reversible "sticker-like" nature. After cracking, the multitude of broken supramolecular bonds located at the newly generated interface recombine by applying external forces and "close the gap", thereby healing the damaged area. Since these non-covalent interactions, largely in thermodynamic equilibrium, can be reversibly broken, supramolecular polymers exhibit promising features such as improved processing ability and self-healing behavior [21]. Amongst the different supramolecular chemistries, those dealing with hydrogen bonds have been largely explored for self-healing polymers [24, 25, 35]. Sijbesma et al. introduced H-bonds into chemically cross-linked networks to enhance preemptive stress relaxation and impart high creep compliances, so that the mechanical stresses can be relieved [11, 36]. Cross-linked networks with reversible H-bonds can also promote delayed elasticity which assists the recovery of neat surfaces after damaging.

In the current study, we incorporated amide motifs, capable of reversible hydrogen bonding, into a covalently cross-linked epoxy-amine network to obtain coatings, combining the good adhesive performance and outstanding mechanical properties of these polymer systems with an additional self-healing behavior (see Scheme 1). Epoxy-amine bulk coatings were obtained by employing a linear di-amine (Jeffamine D-230) and *N*-(5-aminopentyl) acetamide as curing agents of an epoxy resin (Eponex 1510). Jeffamine D-230 provides toughness and impact resistance to the coatings by creating chemical cross-links (covalent bonds) with the epoxy resin, whereas the physical and reversible cross-links (hydrogen bonds) are provided by the second curing agent, acetamide. To the best of our knowledge, the effect of adding extra amide motifs to promote hydrogen bond cross-links into

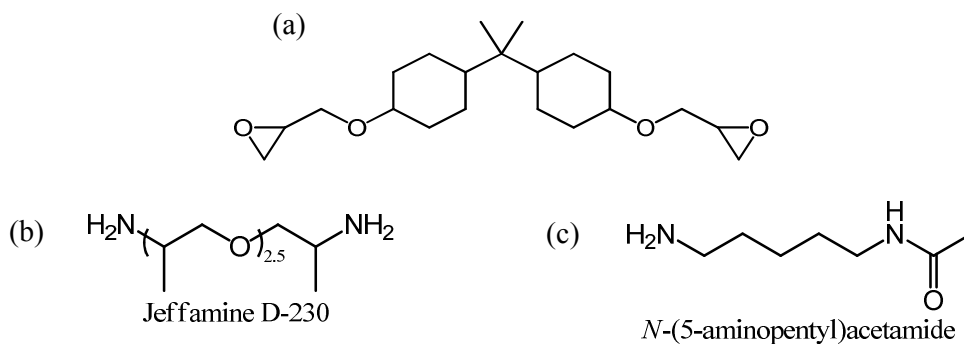
(covalently) cross-linked epoxy-amine coatings and its subsequent self-healing properties have not been reported so far.



Scheme 1. Schematic representation of the macromolecular architectures of the epoxy coatings.

Experimental

Materials. For the preparation of the coatings, hydrogenated DDP epoxy resin (Eponex 1510, Momentive BV) with an equivalent weight (eqw) per epoxide group of 210 g/mol was used (see Scheme 2a). Eponex 1510 is a low viscosity resin, 18-25 P at 25 °C, and will further be denoted as **E** in this paper. The selected curing agents (amines) are Jeffamine D-230 (Huntsman B.V., Belgium; $M_w = 230$ g/mol, NH- $eqw = 60$ g/mol, see Scheme 2b) and *N*-(5-aminopentyl) acetamide (TCI Europe N.V.; $M_w = 144.22$ g/mol, NH- $eqw: 72.11$ g/mol, see Scheme 2c), which will be further denoted as **J** and **A**, respectively. All chemicals were used without any further purification. These raw materials were chosen on basis of their good wet adhesion behavior [7].



Scheme 2. Molecular structure of (a) Eponex 1510 (**E**), (b) Jeffamine D-230 (**J**) and (c) *N*-(5-aminopentyl) acetamide (**A**).

Preparation of the coatings. Coatings were prepared by mixing E, J and A at different molar ratios to investigate the influence of the physical *versus* chemical cross-links ratio on the properties of the matrix. The produced samples are EJ, EJ 5% A, EJ 10% A, EJ 15% A, EJ 20% A and EJ 25% A, where the percentage values written before A refer to the mole percentage of acetamide in the coating. Aluminum 2024-T3 alloy plates ($10 \times 15 \times 0.06 \text{ cm}^3$, ThyssenKrupp Aerospace) were used as substrate. These substrates were pre-treated by using sand paper (Scotch-Brite, 3M), washed with acetone to remove oil and dust, and thereafter dried using a nitrogen flow [7].

After the preparation of the Al substrates, the mixtures of Eponex, Jeffamine D-230 and N-(5-aminopentyl) acetamide were magnetically stirred for 30 min after which a coating was directly applied on the pre-treated Al substrates by utilizing a quadruple film applicator (“Doctor-Blade”) driven by a Master coating apparatus (Erichsen GmbH & Co. KG), at a rate of $10 \text{ mm}\cdot\text{s}^{-1}$ with a “wet” thickness of $120 \text{ }\mu\text{m}$. The curing of the coated substrates was carried out at $100 \text{ }^\circ\text{C}$ for 4 hours and the samples were allowed to cool down inside the oven until it reached room temperature. To prepare larger samples for DMA, DSC, TGA and FTIR measurements, the stirred mixture was casted on thin-wall aluminum cups with a thickness of $\approx 500 \text{ }\mu\text{m}$. Note that the Jeffamine is a di-amine containing two primary amine groups which can each react twice and is considered to be an ideal four-functional cross-linker [37].

Thermal Gravimetric Analysis (TGA). The weight loss and onset of degradation of the cured epoxy-amine coatings were determined using a TGA Q500 (TA Instrument). Samples were prepared by using 10 mg from the material cured in the thin-wall aluminum cups. The samples were heated at rate of $10 \text{ }^\circ\text{C}/\text{min}$ from $25 \text{ }^\circ\text{C}$ to $700 \text{ }^\circ\text{C}$ under a nitrogen atmosphere.

Differential Scanning Calorimetry (DSC). The glass transition temperatures (T_g) of the coatings were determined using a DSC-Q2000 (TA Instruments). Tzero (TA, Switzerland) and Tzero Hermetic Lid (TA, Switzerland) pans were used employing samples of about 3-5 mg. All samples were heated from -90 °C to 150 °C and then cooled to -90 °C at a rate of 5 °C/min. Three heating and cooling cycles were performed on each sample and the T_g was determined from the second heating cycle at the half-height value of the transition in DSC trace.

Fourier Transform Infrared Spectroscopy (FTIR). FTIR measurements were carried out using a Varian 3100-FTIR (Excalibur Series) spectrometer at room temperature in Attenuated Total Reflection (ATR) mode to observe the presence of hydrogen bonds in the epoxy-amine networks. A diamond crystal was used and all the spectra were recorded in the range of 4000 cm^{-1} to 650 cm^{-1} with a resolution of 4 cm^{-1} . On average 100 scans were co-added per spectrum and one average spectrum was recorded for each sample measured after which the average background was subtracted.

Transmission-FTIR studies were performed using a Varian 670-IR FTIR Spectrometer and a hot stage (Linkam cell, TMS 94) at 100 °C. The behavior of the coatings was monitored as a function of time to study the curing kinetics of the epoxy resin in the presence of acetamide. In order to do so, KBr pellets were prepared by placing approximately 150 mg dry KBr powder in a mould (diameter ≈ 10 mm) and applying ≈ 7 ton compression force for 10 min under vacuum. The thus prepared pellets were immediately placed in the oven at 60 °C to avoid moisture absorption.

The KBr pellets were equilibrated at 100 °C for 10 minutes prior to the kinetic experiments. A typical coating formulation was prepared (≈ 1 g) and stirred with a magnetic stirrer for 1-2 min to obtain a homogeneous distribution of the components and a small

droplet was placed in between two KBr pellets. All spectra were recorded *in situ* during the cross-linking reaction, between 4000 and 650 cm^{-1} with a resolution of 4 cm^{-1} . For each composition, 130 spectra (100 scans co-added per spectrum) were taken in time intervals of 30 s. The curing kinetics were analyzed by calculating the area and height of the vibration band at 3050 cm^{-1} , attributed to the C-H stretching of the oxirane ring, which was expected to decrease as Eponex 1510 reacted with the amines.

Transmission-FTIR characterization was also performed to analyze the influence of temperature on the weakening of hydrogen bonds. For that purpose, Eponex 1510, Jeffamine D-230 and N-(5-aminopentyl) acetamide were mixed with a magnetic stirrer for 30 min and 1 small droplet was placed on a ZnSe disc. The samples were left at room temperature until they were completely solidified. Temperature dependent spectra were collected, starting from room temperature until 200 °C with temperature intervals of 10 °C, during heating and cooling ramps. Background spectra were previously recorded at every temperature at which the spectra were obtained and respectively subtracted. All other parameters were the same as for the curing kinetics, as mentioned in the previous paragraph.

Dynamic Mechanical Analysis (DMA). DMA measurements were carried out using a DMTA Q-800 (TA Instruments) to determine the storage modulus E' , the loss modulus E'' and the T_g of the samples. Additionally, stress-strain curves were obtained and creep and stress relaxation was investigated for both the fully covalent and acetamide containing samples.

The elastic modulus measurements were carried out in tensile and multi-frequency strain mode, where the temperature was increased from 0 °C to 150 °C, with a ramp of 2 °C/min and collecting data points every 2 s. Rectangular samples of about 5.3 mm \times 0.5 mm cross section and about 12 mm length were tested at 1 Hz and 15 μm amplitude. The storage

modulus was used to calculate the experimental cross-link density XLD according $XLD = E' / 3RT$ where R and T denote the gas constant and temperature, respectively, and E' denotes the plateau modulus (the minimum point in the $E'-T$ curve). The experimental M_c (molecular mass between cross-links) values were calculated as $M_c = \rho/XLD$ [7]. The glass transition temperature T_g was taken as the temperature with maximum loss angle ($\tan \delta$).

The storage moduli were also calculated after a thermal treatment. For this treatment the samples were heated up from room temperature to 100 °C and cooled down again to room temperature at 5 °C/min and isothermal waiting periods of 1 hour at each temperature. The storage modulus before and after thermal treatment was compared for each composition. Data points were collected every 2 s for the samples having dimensions of $5.3 \times 0.5 \times 12 \text{ mm}^3$ at 1 Hz and 15 μm amplitude (see Supporting Information, SI).

In order to obtain stress-strain curves, samples of $5.3 \times 0.5 \times 12 \text{ mm}^3$ were exposed to a ramped force and the resultant deformation was monitored isothermally, at room temperature and at 100 °C, with isothermal curing times of 5, 30 and 120 min. A 3 N/min force rate was selected with an upper force limit of 18 N and employing a preload force of 0.001 N. The effect of the thermal treatment time on elongation at break and Young's modulus was compared for various samples. For each composition, the measurements at 100 °C were repeated twice, while at room temperature the measurements were repeated five times. Recovery of the strength is evidently important as well. However, at room temperature the materials are in the glassy state (see T_g s in Table 1 and Figures S3 and S4, SI) and the DMA samples are too small for reliable strength measurement.

Creep measurements were done at a stress of 0.1 MPa (linear viscoelastic region) and a creep time of 120 min, followed by a recovery time of 60 min. The samples were tested at 35 °C, 45 °C, 100 °C and 5 °C below the T_g measured for each sample (for T_g s, see Table 4).

Each measurement was performed on two identical specimens to check reproducibility and a preload force of 0.01 N was applied in all cases.

Stress relaxation measurements were conducted at a temperature 5 °C below the T_g measured for each sample (for T_g s, see Table 4). The stress at a constant strain of 2% was monitored for 120 min. Then, the strain recovery was followed for 60 min in the absence of any external stress. Data points were collected every 2 s.

Optical microscopy. The healing process at 45 °C was monitored by optical microscopy using a Reichert-Jung Polyvar-Met microscope equipped with a digital camera. The measurements were performed for 1 hour, with image collection at every minute. Before starting the characterization, a notch of $\approx 100/200$ μm width and 30/60 μm depth was created by a well-defined cutter with a top angle of $\approx 140^\circ$ (BYK Gardner GmbH, PIG Universal) using a 2.3 kg load. In order to show the effect of hydrogen bonding on the healing process, the healed samples were subjected to DMA measurements and the recovery of the mechanical properties was investigated.

Pull-off test. Pull-off measurements, following procedures previously reported [7], were used to identify the adhesion strength of the various coatings to the Al substrate. Three different sets of samples were prepared. The first set was kept in dry conditions at room temperature, the second was immersed in distilled water for one week and the third was dried at 100 °C after 1 week of immersion in distilled water.

For the second set (wet adhesion), the edges of the samples were sealed by water-proof tape (Tesa® tape) before immersion. After immersion, the tape was removed, the samples were wiped with soft (Kimtech) tissue paper, blown dry using N_2 and after that directly tested. For the third set, the same procedure was applied for the immersion. However, after

removing the water-proof tape, the samples were placed inside the oven at 100 °C for 24 hours and kept inside the oven for at least 6 hours at room temperature to make sure they were completely dry.

Before starting the pull-off test, the studs (stainless steel, $d = 8$ mm) were sand-blasted at 2 bar. After sand-blasting, they were rinsed with water to get rid of the larger sand particles, followed by sonication in water for 5-10 min at least 3 times, or until no dust was observed on the studs. The studs were then washed several times with acetone and dried in the oven at 40 °C just before gluing them on the coated Al substrates. For each coating composition, eight panels were cut with dimensions of 2×3 cm². The coated surface of each panel was ground gently by sand paper (#1200, 3M), to enhance the mechanical anchoring of the glue [7]. Thereafter the studs were attached perpendicular to the coated substrates with a glue (3M scotch-weld DP460) which was cured at room temperature for two days. Before starting the pull-off test, the coating and cured-glye around the stud were removed using an electrical drill. The pull-off measurements were carried out using an Easy TEST (EZ 20 Lloyd Instruments) tensile equipment applying a velocity of 1 mm/min. The force required to detach the coating from the substrate was monitored as a function of the stud displacement. A schematic of the pull-off measurements is presented in Figure S6 (see SI) [7].

Results

Thermal properties of the coatings. The influence of acetamide incorporation on the thermal properties of the epoxy-based coatings was investigated using TGA, DSC and DMA. TGA showed that all the coatings are stable up to ≈ 250 °C (for TGA curves, see Figure S1 in the SI). Therefore, the DSC measurements were carried out by heating the samples until maximally 150 °C to prevent possible degradation.

Figure 1a shows the DSC thermograms of the various epoxy coatings. In comparison with

the fully covalent network, a slight decrease in T_g up to maximally of ≈ 5 °C was observed for the samples cured with 25 mole % of acetamide. Figure 1b shows the DMA $\tan \delta$ curves from which it can be observed that the T_g values taken from $\tan \delta$ are 10-15 °C higher than the T_g s taken from DSC, in agreement with literature results. The main reason for this difference is that these techniques probe different aspects of the glass transition as reported in the literature [38]. Moreover, these transitions are more easily detected by DMA than by DSC since mechanical changes are typically more dramatic than changes in the heat capacity [38]. Table 1 summarizes all the thermal data of the various samples. From this table it can be concluded that the T_g of the coatings decreases slightly by the incorporation of the acetamide.

Table 1. Thermal characterization of epoxy coatings.

Epoxy resin	Curing agent (molar ratio)		Ratio (E/NH)	Onset of degradation (°C)	T_g^1 (°C)	T_g^2 (°C)
	J D-230	A				
Eponex 1510	1	0	1:1	≈ 266	52	62
	0.95	0.05	1:1	≈ 233	46	61
	0.90	0.10	1:1	≈ 212	47	60
	0.85	0.15	1:1	≈ 254	48	60
	0.80	0.20	1:1	≈ 254	45	58
	0.75	0.25	1:1	≈ 279	44	57

Note: T_g^1 is the glass transition temperature based on DSC and T_g^2 is determined using DMA.

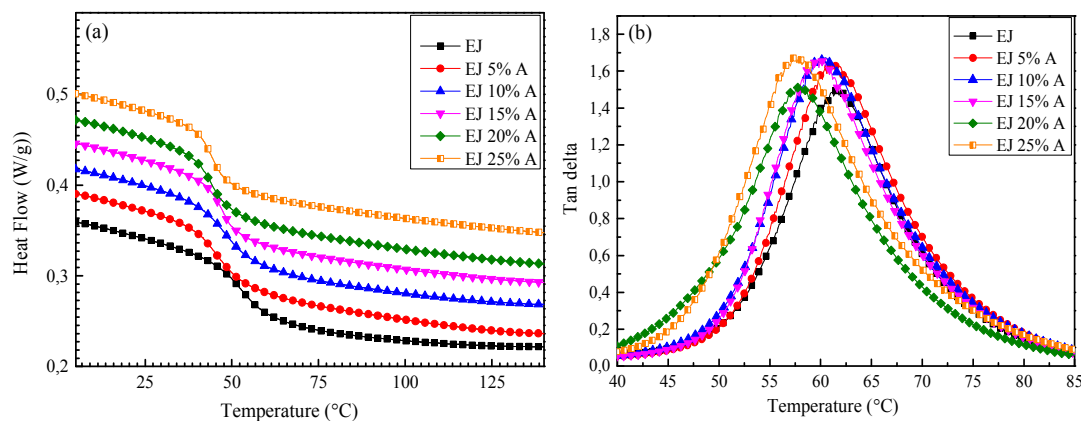


Figure 1. (a) DSC thermograms (2nd heating run); (b) $\tan \delta$ values taken from DMA data.

Molecular characteristics of coatings. The coatings prepared with different acetamide percentages (% A) were characterized by ATR-FTIR to obtain a molecular perspective of the samples and to verify the existence of hydrogen bonding in the cross-linked network. The changes in specific vibration bands responsible for inter/intra molecular hydrogen bonding are depicted in Figure 2, while Table 2 shows the peak assignment of the various coatings as described by their intensity and absorption frequencies.

Table 2. The characteristic ATR-FTIR absorption frequencies of the EJ(A) coatings [39, 40].

Vibrational mode	EJ		EJ 5% A		EJ 10% A		EJ 15% A		EJ 20% A		EJ 25% A	
	I	Wn (cm ⁻¹)	I	Wn (cm ⁻¹)	I	Wn (cm ⁻¹)	I	Wn (cm ⁻¹)	I	Wn (cm ⁻¹)	I	Wn (cm ⁻¹)
O-H str and non-H-bonded N-H str overlap	b, m	3404	b, m	3398	b, m	3368	b, m	3364	b, m	3356	b, m	3345
C-H str (oxirane group)	a		a		a		a		a		a	
C-H of CH ₂ and CH asym str	s	2929	s	2931	s	2930	s	2929	s	2930	s	2930
C-H of CH ₂ and CH sym str	s	2859	s	2860	s	2860	s	2859	s	2859	s	2859
C=O str (Amide I)	a		w	1653	w	1652	w	1652	m	1652	m	1652
N-H bending	w	1645	a		a		a		a		a	
C-N str and C-N-H bending-in-plane (Amide II)	a		w	1552	w	1553	w	1554	w	1553	w	1553
C-H deformation of CH ₂ and CH ₃	s	1447	s	1447	s	1447	s	1447	s	1447	s	1446
CH ₃ deformation of C-(CH ₃) ₂	m	1367	m	1367	m	1367	m	1367	s	1367	s	1366
C-O-C stretching of ethers	s	1090	s	1089	s	1088	s	1088	s	1088	s	1088
C-O str (oxirane group)	w	909-915	w	901	w	901	w	901	w	901	w	901

Note: The intensity I is indicated by w = weak, m = medium, s = strong, b = broad and a = absent, while the mode labels are str = stretching, asym = asymmetric and sym = symmetric, Finally, Wn denotes Wave number.

The oxirane ring has characteristic absorptions at 915 cm⁻¹ and 3050 cm⁻¹ which are attributed to C-O and C-H stretching vibrations, respectively. Figure 2a shows that peaks associated with these bands are absent, indicating the full consumption of the epoxy groups during the curing reaction and the formation of chemical cross-links in the system, as far as can be judged by FTIR.

The presence of hydrogen bonding can be identified by its signature wavenumbers at 3300 cm⁻¹ (N-H stretching) and 1650 cm⁻¹, attributed to hydrogen-bonded C=O stretching (Amide I). For the EJ coatings without any acetamide addition, the C=O stretching bands

Amide I at $\approx 1652 \text{ cm}^{-1}$ and Amide II at $\approx 1552 \text{ cm}^{-1}$ are obviously absent, so that the small peak at 1645 cm^{-1} is probably due to the N-H bending vibration of some unreacted Jeffamine. The introduction of acetamide into the cross-linked network provides the formation of hydrogen bonds [41]. Hence, when acetamide is incorporated in the coatings, the presence of the stretching bands of Amide I and Amide II groups becomes visible.

The sample without acetamide shows a band at 3404 cm^{-1} which may be assigned to O-H stretching vibration. Since non H-bonded N-H stretching is also observed around 3400 cm^{-1} , overlapping of these two vibrational bands is likely to occur. As amide motifs are incorporated into the system, the peak between $3400\text{-}3300 \text{ cm}^{-1}$ starts to broaden. For EJ 25% A the center of this broadened peak is observed at 3345 cm^{-1} . At first glance, this broadening could be interpreted as the result of an overlapping of the O-H stretching, non H-bonded and H-bonded N-H stretching. However, it may be speculated that the incoming of N-H stretching (H-bonded) causes the shift from 3404 cm^{-1} for EJ, to 3345 cm^{-1} for EJ 25% A. These results are a good indication of the presence of hydrogen bonds in the networks of the cross-linked systems containing acetamide.

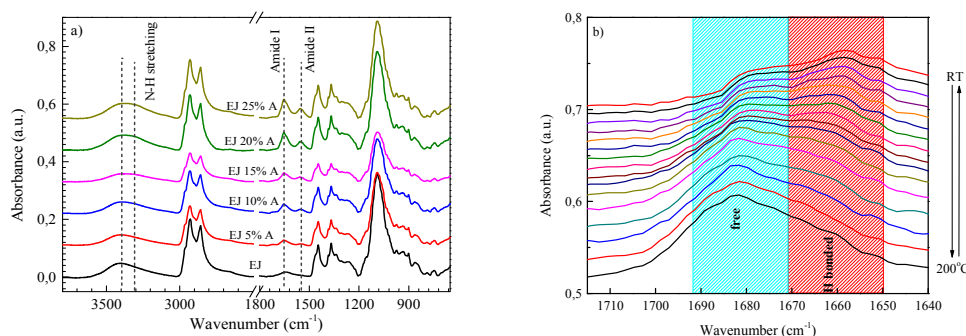


Figure 2. (a) ATR-FTIR spectra of the various coatings. (b) Transmission-FTIR measurements showing the effect of temperature on the weakening of hydrogen bonds for coating EJ 25% A on heating/cooling with a rate of $10 \text{ }^\circ\text{C}/\text{min}$ from RT to $200 \text{ }^\circ\text{C}$.

Temperature dependent transmission-FTIR measurements were carried out to analyze the influence of temperature on the weakening of hydrogen bonds. Figure 2b depicts the changes in the peak positions of Amide I signals for EJ 25% A.

The amide I mode (\sim carbonyl stretch) is sensitive to order [42] and the contributions to the band envelope, assigned to "free" (non-hydrogen bonded) carbonyl groups, together with ordered and disordered hydrogen bonded carbonyl groups, are readily discerned. As the three different contributions comprising the amide I mode have similar absorptivity coefficients [42], the change in hydrogen bonding can be relatively easily followed.

At room temperature, Amide I bands are observed at 1654 cm^{-1} , in agreement with the values obtained from ATR-FTIR measurements. As the temperature is increased, the signature wavenumber at 1654 cm^{-1} , attributed to hydrogen bonded C=O stretching, shifts to higher frequencies and at $50\text{-}60\text{ }^{\circ}\text{C}$ a partial weakening of hydrogen bonds can be already identified. At $100\text{ }^{\circ}\text{C}$ the signature band is observed at 1672 cm^{-1} and shifts further to 1681 cm^{-1} at $200\text{ }^{\circ}\text{C}$, which is a typical value for non H-bonded carbonyl stretching vibrations. The large shift of the Amide I signal to higher frequencies is a clear sign of hydrogen bond weakening. Furthermore, as the sample is cooled down from $200\text{ }^{\circ}\text{C}$ to $40\text{ }^{\circ}\text{C}$, the wavenumber attributed to the Amide I signal shifts back to lower frequencies. In the cooling cycle, the wavenumber decreased from 1681 cm^{-1} ($200\text{ }^{\circ}\text{C}$) to 1668 cm^{-1} at $100\text{ }^{\circ}\text{C}$, which is very similar to the 1672 cm^{-1} at $100\text{ }^{\circ}\text{C}$ of the heating cycle. Moreover, the wavenumber assigned at $40\text{ }^{\circ}\text{C}$ of the heating cycle is 1658 cm^{-1} and of the cooling cycle is 1657 cm^{-1} . This similarity of wavenumbers at the same temperature during the heating and cooling shows that the hydrogen bonds, by their nature, weaken at elevated temperatures but reform again as the temperature decreases.

Transmission-FTIR was also used to monitor the curing kinetics of the coatings as a function of time. The peak absorbance at 3050 cm^{-1} , associated with the C-H stretching of the

oxirane ring, was followed for 120 min to understand how cross-linking proceeds as a function of time. Figure 3a shows the decrease in the peak absorbance values of EJ 25% A between 0-120 min. The other compositions showed very similar trends in terms of the decrease in absorbance values (not shown).

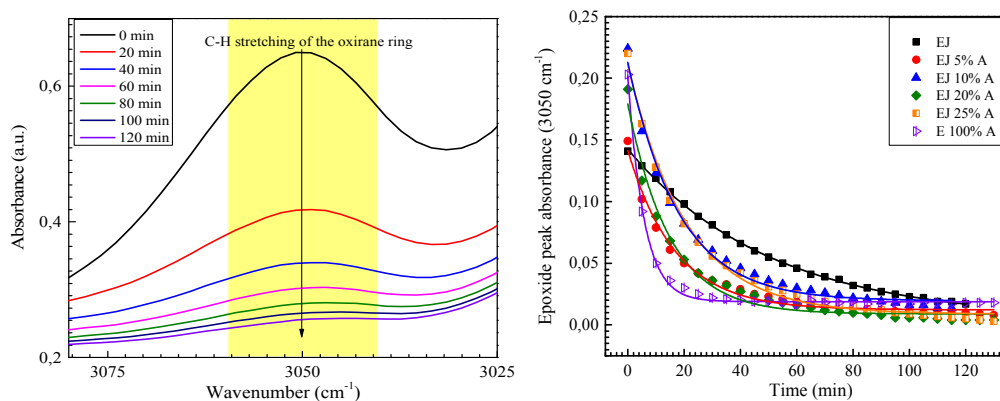


Figure 3. (a) The IR peak absorbance of EJ 25% A at 3050 cm^{-1} between 0-120 min. (b) Epoxide IR peak absorbance based on height at 3050 cm^{-1} for all compositions.

The 909 cm^{-1} or 3050 cm^{-1} absorption bands, corresponding to the C-O stretching vibrations of the epoxy group and to the C-H stretching of the oxirane ring respectively, have been used by many researchers to follow and analyze the curing kinetics of epoxy-amine systems [40]. Here the extent of cross-linking was determined by the peak areas of the epoxy group absorbance at 3050 cm^{-1} [40]. The absorbance values were plotted as a function of time in order to determine the rate of curing (Figure 3b). A steep decrease in slope was observed in the first 30 min for all compositions, indicating a high rate of consumption of epoxy groups and therefore a high curing reaction rate. Due to the mobility of the monomers or low molar mass material (dimers, trimers, etc.) formed, a high rate is expected initially. However, the rate of cross-linking decreased significantly after 30 min, due to the restricted mobility of the higher molecular weight, partially cured epoxy network [40].

Structural characteristics of the networks. In order to gain a deeper insight into the structural characteristics of the cross-linked networks and determine the influence of amide motif incorporation, DMA measurements were carried out to determine the storage modulus E' , the loss modulus E'' and $\tan \delta$ as a function of temperature for all cross-linked coatings (Figure 4). The moduli values were used to calculate the cross-link densities. Table 3 shows the XLD values and the corresponding molecular mass between cross-links.

Table 3. Cross-link density values for the various coating compositions.

	XLD (mole/cm ³)	M_c (g/mole)
EJ	7.3×10^{-4}	1370
EJ 5% A	5.6×10^{-4}	1790
EJ 10% A	6.0×10^{-4}	1670
EJ 15% A	5.4×10^{-4}	1850
EJ 20% A	5.5×10^{-4}	1820
EJ 25% A	3.9×10^{-4}	2560

The highest cross-link density (XLD) was found for sample EJ without amide motifs while the incorporation of 25 % amide motifs (EJ 25%A) caused a two-fold decrease in XLD values. Therefore, we conclude that the addition of acetamide into the epoxy network increases the ratio of physical to chemical cross-links but also decreases the overall cross-link density. The M_c calculations were done using Flory's relations for non-conforming polymer networks because more sophisticated methods, such as that of Miller and Makosco [43] or Lesser and Crawford [44] can only be used when the effective functionality and some other data are known, which is generally (and also here) not the case. However, an estimate based on these methods learns that the reported M_c values are about twice that expected but that the trend is not affected. Since the comparison is qualitative only, the simple theory of rubbery elasticity for M_c considerations was used.

Dissolution tests with the EJ and EJ 25% A material in THF, water, acetone and ethanol, using 10 mg material per 1 ml solvent (total volume typically about 5 ml) showed no dissolution after 5 days. The degree of swelling with acetone was about 25% for both the EJ and the EJ 25% A material, while after drying for 24 h at 40 °C, the decrease in weight for both materials was less than 1%. This confirms the stability of these materials after prolonged contact with solvents that potentially could dissolve the constituting components.

Mechanical properties of the films. In Figure 4 the evolution of the tensile storage moduli (E') with temperature is illustrated for all samples. It can be observed that the storage modulus of the material at room temperature does not change significantly after incorporation of the amide motifs. The modulus of the EJ sample is ≈ 2080 MPa while that of EJ 25% A has the value of ≈ 2020 MPa. Furthermore, the moduli of samples with a lower mole % of acetamide changed also only about 2-3 %.

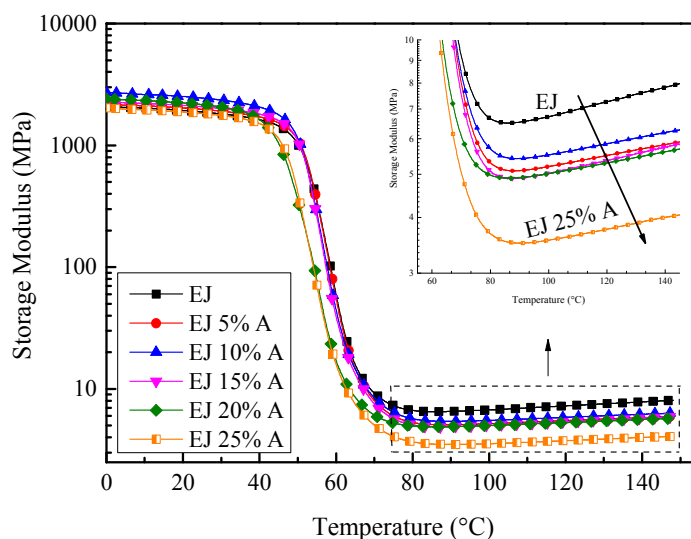


Figure 4. Influence of incorporation of amide motifs on storage modulus.

In fact, more pronounced effects of incorporating amide motifs were observed in the plateau modulus above T_g . The plateau modulus (measured at 86.4 °C) of EJ is 6.5 MPa, whereas EJ 25% A showed a value of 3.5 MPa (measured at 89.6 °C). It should be recalled that at this temperature, the weakening of the hydrogen bonds has already set in, as discussed above when dealing with the FTIR results, and that this weakening has an impact on the storage moduli. Above 80 °C, the storage moduli exhibit a slight increase for all compositions. This is most likely related to the entropic stiffening of the system due to an increase of the temperature [45], although the thermal treatment (see SI for thermal treatment effect considerations, Figure S2 and S3) and the presence of water may have a minor influence [46].

Creep/Stress Relaxation Measurements. The analysis of the various samples in terms of thermal and mechanical characteristics showed the effect of the incorporation of the amide motifs on the rubber plateau modulus, that is, the cross-link density, and the effect of the thermal treatment. This analysis suggests a different relaxation of applied stresses for the materials having a different content of amide motifs. Therefore, the effect of hydrogen bonding was evaluated in terms of creep and stress relaxation.

Figure 5 shows the creep behavior of samples that were subjected to 0.1 MPa applied stress for 2 hours at different temperatures and then allowed to recover for another 60 min. When measured at 100 °C (Figure 5a), far above T_g , the material EJ 25% A – with the highest amide content – shows the highest equilibrium elongation result while the fully covalent material EJ shows the lowest. After stress removal, only EJ exhibits almost complete strain recovery and the fast and instantaneous response of the covalent network indicates almost fully elastic behavior. With increasing acetamide content, a slower relaxation and a higher

residual strain after stress removal were observed. As more amide motifs were incorporated into the networks, an increasingly incomplete strain recovery was obtained.

Measurements were also performed at a fixed temperature difference of 5 °C below the T_g of each material (Table 4). At 5 °C below T_g , the material EJ 25% A is elongated up to a strain of 3.7 %, whereas for the fully covalent network EJ the strain is 1.9 %.

At 5 °C below the T_g (Figure 5b) material EJ fully recovers its original dimensions at a (relatively) fast rate, after stress removal while the acetamide containing materials exhibit a slightly slower rate and less strain recovery. The main reason for this slow relaxation could be irrecoverable creep introduced by the non-covalent bonds.

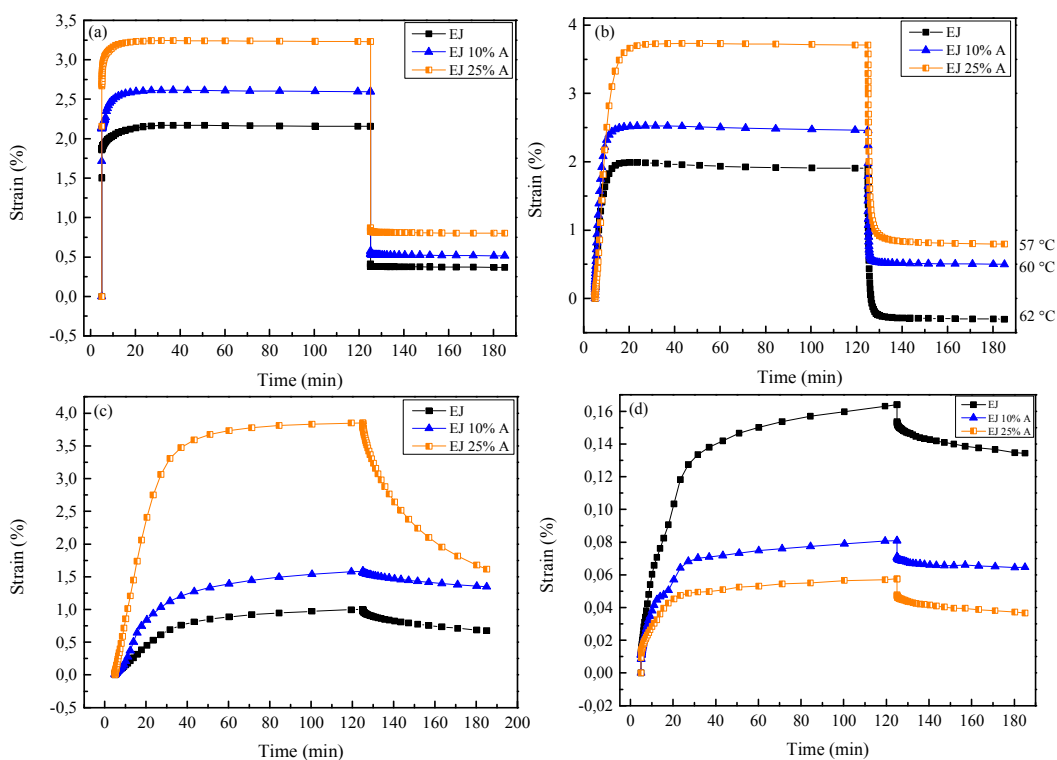


Figure 5. Creep measurements at 0.1 MPa stress at (a) 100 °C, (b) 5 °C below each material's T_g , (c) 45 °C, and (d) 35 °C.

A similar behavior was observed for the creep experiment at 45 °C of the EJ 25% A sample (Figure 5c). This sample elongated up to a strain of 3.7 %, whereas EJ and EJ 10% A samples elongated to 1.0% and 1.6%, respectively. When the stress is removed, the recovery is slower for all the samples as compared to room temperature, in particular for EJ and EJ 10% A. Moreover, full recovery to original state was not observed at this temperature, for any of these materials.

In the glassy state, at 35 °C (Figure 5d), the creep measurements exhibit a reversed behavior as compared higher temperatures. Since the temperatures are approximately 25 °C below the T_g for each of the samples, very small final strains were observed. The fully covalent material exhibits 0.2% of final equilibrium strain after 120 min of creep, whereas EJ 25 % A shows 0.01% after the same time. In this case the recovery is much slower and irrecoverable creep is observed. In addition, it should be noticed that the rate of creep is also slower for all H-bonded samples than for the fully covalent networks.

Besides creep measurements, stress relaxation experiments were performed in order to investigate the relaxation of stresses in greater depth. Figure 6a illustrates the stress at a constant strain of 2% monitored during 120 min and Figure 6b shows the strain recovery followed for 60 min in the absence of any external stress. For the fully covalent network, the stress required to maintain the material at 2% constant strain decayed with time, starting at a value of 2 MPa and equilibrating at 0.083 MPa. As the amount of acetamide is increased, the materials can be kept at the same strain with a lower stress, 0.03 MPa for EJ 25% A (Figure 6a). Furthermore, the acetamide containing samples show incomplete strain recovery to about 1.1%, whereas the fully covalent cross-linked samples recovered to about 0.5% (Figure 6b).

Deformation by creep will introduce local, internal stresses in the material. When the internal resistance to recovery is too large with respect to the driving force (the local internal stresses), the reflow will stop before zero deformation is reached. Also, when the driving

force is low (low internal stresses due to easy rearrangement of the chains), the recovery will stop before zero deformation is reached. Recent work by Zhang et al. [30] using systems with rather stiff cross-linkers and, hence, providing a relatively high driving force, show recovery within a couple of hours after 7 days straining at 100%. In our case, we used Jeffamine as cross-linker, which is known for its flexibility, and this probably results in a too low driving force for full recovery. Generally, a slower stress relaxation of networks below T_g might be related to a large amount of defects (e.g., dangling and non-connected chains) in the structure, as has been discussed (See, e.g., [47]), but the presence of defects cannot explain the inversion of the creep behavior below and above the T_g .

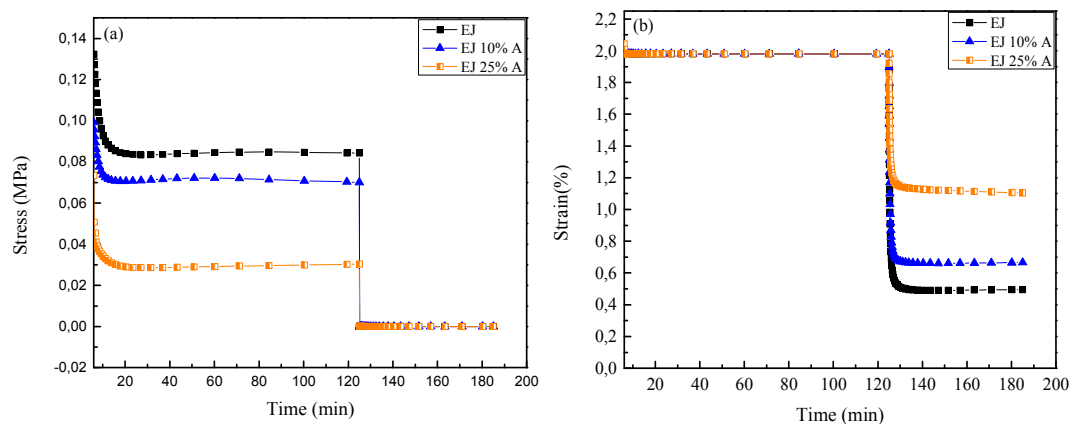


Figure 6. Stress relaxation measurements at 5 °C below the T_g of films EJ, EJ 10% A and EJ 25% A: (a) stress as a function of time at 2% constant strain, (b) strain (%) as a function of time for the same experiment showing the strain recovery for 60 min.

To quantify the time-dependent behavior observed with creep and recovery experiments, the experimental curves of creep at 35 °C were fitted by means of the Burgers model [48], as shown in Figure S5 (see SI). The non-linear curve fit function of the OriginPro 7.5 software was used to obtain the four parameters k_M , k_K , η_M and η_K . As shown in Figure S5, the model fits the experimental data well. The values of the four parameters are summarized in Table S2. As can be seen from the fitting results, the value of the parameter η_M , associated with the viscosity of the Maxwell dashpot, increases with increasing acetamide content. This reflects the slower increase of strain during the loading period with increasing acetamide content.

Moreover, while the Maxwell stiffness k_M is approximately constant, the Kelvin stiffness k_K and viscosity η_K increase with increasing amide content, signifying the introduction of delayed elasticity.

Self-healing behavior. To assess the degree of self-healing of the coatings, a notch of width $\approx 200 \mu\text{m}$ and depth $\approx 60 \mu\text{m}$ was created with a well-defined cutter on the material with composition EJ 25% A (see experimental) and examined by optical microscopy. The progress of self-healing was monitored for 1 hour with 10 min intervals. Figure 7 shows the initial and final surface of both the EJ and EJ 25% A material. More images showing the progress of self-healing for EJ 25% A and EJ are reported in the SI, (Figures S7, S8 and S9).

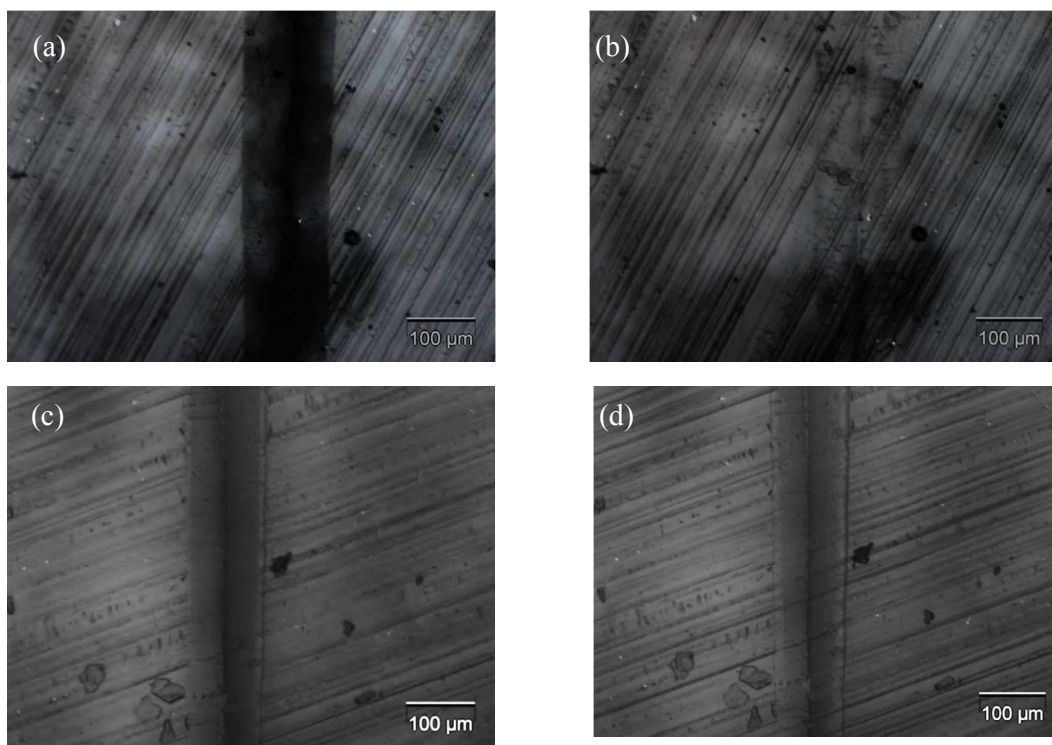


Figure 7. Optical microscope images of the center of a notch showing the healing process at temperature T as a function of time after the notch is formed: (a) EJ 25% A, 0 min; (b) EJ 25% A, 10 min; (c) EJ, 0 min; and (d) EJ, 60 min. For EJ 25%, $T = 45 \text{ }^\circ\text{C}$ and for EJ, $T = 49 \text{ }^\circ\text{C}$ (in both cases $12 \text{ }^\circ\text{C}$ below the T_g of the material, see Table 1).

The material containing the largest amount of acetamide motifs (EJ 25% A) shows complete healing in 10 min at 45 °C (12 °C below T_g , Figure 7a and 7b), probably caused by the delayed elasticity introduced by the physical cross-links. The reference material having only covalent cross-links (EJ) was also tested applying the same procedure at 49 °C (also 12 °C below T_g). Figure 7c and 7d show that even after 1 hour the notch was not healed at all, as expected. The progress of self-healing at 45 °C was also monitored by determining the depth and width of a notch as function of time on a cross-section of EJ 25% A for 1 hour with 1 min intervals. Quantitative data are provided in the SI (Figure S10).

For a self-healing system not only the healing of the damage, but also the recovery of the initial mechanical properties is of great importance [14]. Therefore, the moduli of both samples after healing were measured with DMA. Figure 8 presents a comparison of the storage modulus as a function of temperature for samples before and after healing. A summary of the characteristics is given in Table 4.

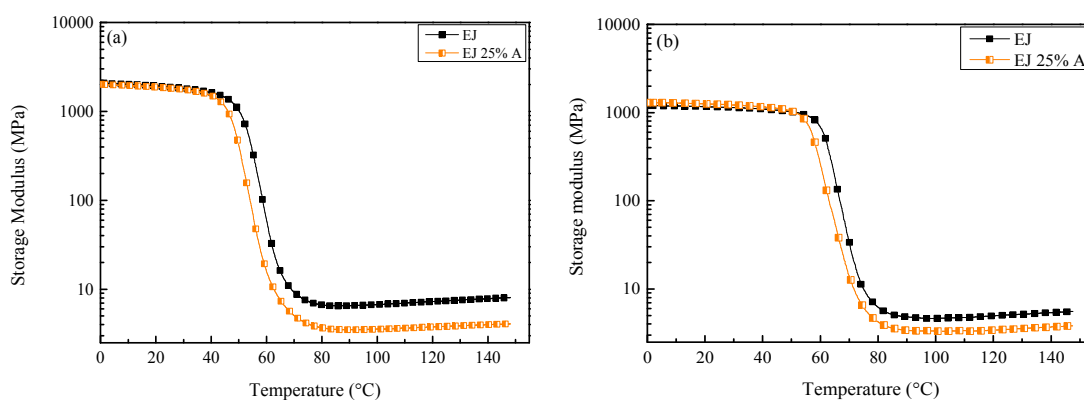


Figure 8. Storage modulus as a function of temperature for EJ and EJ 25% A: (a) pristine material and (b) after notching and healing experiments.

To our surprise, the T_g after healing increased by about 15 °C for both the EJ and EJ 25% A materials. The main difference in history of these materials before and after healing is their exposure to moisture. While the pristine materials were exposed to ambient conditions for at

least several days, the healed materials were after healing within half an hour transferred to the DMA apparatus. This suggested a significant influence of water on the properties. Hence, humidity (RH) controlled-DMA (dynamic mechanical analysis) experiments under different controlled humidity levels were performed. These experiments (SI, Figures S11 and S12) showed a fast uptake and release of water, in fact most of the moisture was exchanged within 30 to 60 min (see Table S3). They also indicated a decrease in T_g of about 10 °C by changing the RH from about 10% to 60%, combined with a decrease in modulus by a factor of one and a half to two in 30 to 60 min. The water uptake effect on epoxy resins, both from solutions or just from air humidity, is known since a long time, has been studied extensively and introduces a plasticizing effect [49], [46], [50]. This absorption is mainly associated with the polar centers of the resin, namely tertiary amines or hydroxyl groups formed in the polymerization process, and varies with, e.g., cross-linking agent and curing conditions (temperature and humidity) [51], [52]. Similarly, the PEO units in the Jeffamine are potentially hygroscopic, and hence also could influence the T_g . In our case the rate appears to be rather high. Although the change in modulus due to moisture is apparent, the change in modulus due to the introduction of acetamide is significantly larger.

After notching followed by the healing experiments, the storage modulus at room temperature shows about a two-fold of decrease for both the EJ and the EJ 25% A materials. While this may seem a noticeable difference, one should keep in mind that minor differences in size for this sample geometry will have a clear influence. Moreover, a much larger cracked area as compared to the notch cross-section might be present (although not observed) which would decrease the modulus observed. When the temperature is increased beyond T_g , the storage modulus reaches exactly the same initial value of 3.5 MPa for EJ 25% A, while the modulus for EJ decreased from 6.5 MPa (pristine material) to 4.6 MPa (after healing).

Table 4. The storage modulus values of EJ and EJ 25% A materials when they are pristine and after the healing trials.

sample	Pristine material		After healing	
	Starting modulus (MPa)	Rubbery plateau modulus (MPa)	Starting modulus (MPa)	Rubbery plateau modulus (MPa)
EJ	2080	6.5	1083	4.6
EJ 25% A	2020	3.5	1291	3.5

Adhesion strength in dry and wet conditions. In order to analyze the influence of the incorporation of H-bonds at the coating-substrate interface and its effect on adhesion strength, pull-off tests were performed in dry, wet and dried-after-wet conditions. For each composition, 8 samples were measured and the average value was taken, as shown in Table 5.

In dry conditions, the fully covalent network displays an average adhesion strength of 9.4 MPa. All of the measured values are in between 7.1 and 10.7 MPa. For a similar fully covalent epoxy network, Meis *et al.* [7] observed an average of 10.1 MPa with a range of 6-12 MPa and a sample standard deviation of ± 1.8 , which is in agreement with our study. The 25 mole % addition of acetamide slightly lowers the average adhesion strength on dry conditions from 9.4 to 7.6 MPa.

Table 5. Pull-off results for different compositions where [] indicates the sample standard deviation (\pm).

Sample name	Dry (MPa)	One week wet (MPa)	Dried, after 1 week wet (MPa)
EJ	9.36 [± 1.07]	6.96 [± 0.90]	8.27 [± 1.38]
EJ 10% A	7.95 [± 0.83]	7.41 [± 0.92]	7.82 [± 1.02]
EJ 20% A	7.98 [± 0.55]	7.71 [± 1.28]	8.42 [± 0.64]
EJ 25% A	7.62 [± 0.85]	7.77 [± 1.39]	8.02 [± 0.69]

In wet conditions, the decrease in pull-off strength is very pronounced for fully covalent coatings as compared to the coatings containing acetamide. For the EJ coatings, the average

adhesion strength decreases from 9.4 to 7.0 MPa. Surprisingly, the coatings having hydrogen bonds showed outstanding wet resistance. With increasing acetamide content, the wet strength decreases by only ≈ 0.6 MPa for the EJ material to ≈ 0 MPa for the EJ 25% A material.

To check whether it is possible to recover the strength after 1 week of immersion in water, the samples were dried in oven at 100 °C for 24 h and left in the oven to cool down for few hours. For the coating with chemical cross-links only (EJ), drying after the immersion period, showed an almost complete recovery of the pull-off strength with a slightly larger error margin (8.3 ± 1.4 MPa). For the samples having acetamide motifs, drying the after immersing in water, showed complete recovery. The average pull-off values changed from 7.7 to 8.4 MPa and 7.8 to 8.0 MPa for 20% and 25% acetamide containing samples, respectively.

Discussion

The glass transition temperature provides information on cross-linking and mechanical properties of polymer networks [53]. The incorporation of amide motifs – H-bonding moieties – in our epoxy-amine cross-linked systems decreases the T_g s with about 5 °C from the fully covalent material (EJ) to the materials containing the largest amount acetamide (EJ 25% A) (Figure 1). The effect can be attributed to the reduced stiffness of the system due to presence of hydrogen bonding and the consequent reduction of the number of chemical cross-links [54].

To confirm the incorporation of the amide motifs and the formation of physical cross-links, ATR-FTIR experiments were performed. As acetamide was incorporated as curing agent, the Amide I and Amide II vibrational bands were observed. Moreover, Amide I was identified at ≈ 1650 cm^{-1} , a typical value for hydrogen bonded C=O stretching. A reversible

behavior as a function of temperature, in terms of shifting of the wavenumber of absorption, was observed for this vibrational band (Figure 2b). Hence, from the FTIR analyses it was concluded that with increasing temperature the H-bonds weaken gradually, but decreasing the temperature strengthens them again.

The addition of acetamide into the epoxy network increases the ratio of physical to chemical cross-links due to the incorporation of amide motifs. However, the use of acetamide as additional curing agent also influences the chemical cross-link density. As Jeffamine D-230 has two di-functional end groups, the addition of acetamide decreases the number of functional groups able to form chemical cross-links. Consequently, the number of chemical cross-linkers decreases, leading to an increase in the average molecular mass between cross-links and a decrease in XLD (Figure 4, Table 3).

The lowest plateau modulus was observed for the sample having the highest mole percentage of acetamide in the system (Figure 4). The properties of these materials are affected by both chemical cross-links and physical cross-links at lower temperatures, whereas at high temperatures only the chemical cross-links are determinant due to the weakening of the hydrogen bonds, [41] as demonstrated by the temperature dependent FTIR measurements (Figure 2).

The general conclusion is that the chemical cross-links play a major role in the determination of storage modulus values at temperatures above T_g , and that the plateau modulus of the coatings can be tuned by varying the cross-link content. At these temperatures, the weakening of physical cross-links may also have a pronounced impact on the thermo-mechanical properties. The slight increase in modulus values at elevated temperatures is probably related to entropic stiffening (Figure S3), although the thermal treatment and presence of water may play a minor role.

The mechanical properties of the epoxy-amine coating network can be considered to be the result of a combination of elastic behavior mainly due to the covalent or chemical cross-links and viscous behavior mainly due to the non-covalent or physical cross-links, introduced by the incorporation of the amide motifs. Below T_g , the different ratio of physical *versus* chemical cross-links is responsible for the difference in creep behavior, rate of creep and recovery as observed for the different samples studied.

The physical cross-links show dissociation and recombination enabling the hydrogen bonds to find a different bonding partner under stress, thereby resulting in a lower elongation. For preemptive relaxation of stresses in coatings, this creep behavior, just below T_g , is of particular interest. The combination of a largely elastic component from the covalent network and a viscous component introduced by the dissociation and recombination of hydrogen bonds explains the lower elongation and lower rate of creep [11, 36] at 35 °C, i.e., below T_g (Figure 4). A similar effect was previously reported by Wietor *et al.* [11] while incorporating quadruple H-bonding Ureidopyrimidone (UPy) moieties into Poly(caprolactone) and Poly(lactic acid) based films. In that case, however, a much larger effect was observed, because in that system it is possible to incorporate a much larger amount of hydrogen bonding moieties.

Above T_g , a reversed behavior was observed and the maximum final strain was obtained for EJ 25 % A, which may be attributed to having a lower covalent cross-link density and almost complete weakening of the H-bonds at 100 °C and thus leading to larger elongation (Figure 4). In addition to creep, stress relaxation measurements were performed at 5 °C below T_g for each of the epoxy-amine samples. In agreement with the creep measurements, the incorporation of hydrogen bonds into the coatings allows for an effective relaxation of the stresses. Close to or above the T_g , the weakening of H-bonds will impart chain mobility leading to the capability of healing superficial damage. Actually, the presence of hydrogen

bonds provides sufficient mobility to fully recover the surface at temperatures just below or above T_g [14, 55]. The lower chemical cross-link density of EJ 25% A allows a better mobility of the network, thereby recovering the damage in a very short time at temperatures even below T_g . For the fully covalent sample the scratch did not heal even after long period of heating at $T_g - 12$ °C (Figure 8 and Table 4). A network with reduced chain stiffness requires mild temperatures beyond T_g to realize enough flow to fully recover the surface after scratching, yet preventing spontaneous sagging [14]. Lafont et al. [56], by changing the molecular weight between cross-links in a polysulfide based thermoset rubber, found that a slightly shorter linkage but with higher flexibility (EPS25) leads to lower T_g and faster healing at the same healing temperature, independently of the thiol-based cross-linker used (Fig. 5) and suggest that the larger $T_{\text{healing}} - T_g$, the faster the healing kinetics.

The modulus values of both EJ and EJ 25% A samples were also evaluated after damage and healing (Figure 8). As expected, the storage modulus of EJ 25% A presents a less pronounced decrease as compared with the fully covalent sample, confirming the healing nature of acetamide containing epoxy-amine materials.

To determine the influence of the addition of acetamide on the adhesion strength, pull-off tests were performed in dry, wet and dried-after-wet conditions. The pull-off strength of the fully covalent network as well as the hydrogen bonded network materials, remain fairly constant with no noteworthy differences between dry or wet condition tests. Since the density of hydrogen bonds incorporated into our system is not really high, the probability of donor and acceptor finding each other is relatively low and, hence, probably insufficient to supply a remarkable change at the interface. For the materials in which high hydrogen bonding efficiency is provided by microstructure modification [57], it is much easier to create such a difference at the interface. Consequently, this may be a way to further improve the current H-bonded epoxy systems and eventually achieve a reversible adhesion recovery state.

Conclusions

In this paper, an epoxy-based coating with tunable hydrogen bonds was successfully prepared and investigated. The incorporation of 25 mole % of H-bonding moieties into the covalent networks created an approximately 5 °C decrease in T_g , a two-fold decrease in cross-link density as well as plateau modulus, and led to higher creep compliances and creep rates, as well as to higher stress relaxation just below T_g . These features, introduced by the acetamide in the epoxy-amine coatings, suggest preemptive healing behavior which helps to reduce the internal stresses arising during the curing of the coating. Furthermore, the samples having 25 mole % acetamide exhibited a complete healing of about 100/200 μm wide and 30/60 μm deep notches in less than 10 min at 45 °C. The physical cross-links allow enough flow to fully recover the damaged surface and providing a recovery of the initial mechanical properties.

The adhesion strength experiments indicated that the fully covalent network and the hydrogen bonded network did not show a pronounced difference in strength under dry conditions and maintain extreme good wet adhesion after 1 week of immersion in water. Hence the introduction of reversible physical cross-links does not have any detrimental effect on the good adhesion properties of the epoxy-amine coatings.

In conclusion, the introduction of hydrogen bonds on epoxy-amine coatings (Eponex 1510-Jeffamine D230) impart a superior relaxation of the mechanical stresses and promotes flow, at temperatures just below T_g , which assists the self-healing of mechanical damage. With these approach we introduce a self-healing behavior in a type of coatings already largely used in industrial applications, without sacrificing their original properties, such as good adhesion to metal substrates.

ASSOCIATED CONTENT

Supporting Information.

The Supporting Information contains data concerning the thermal stability of the epoxy-amine coatings and more detailed information on materials mechanical properties.

AUTHOR INFORMATION

Corresponding Authors

* E-mail: M.V.Villani@tue.nl; G.deWith@tue.nl;

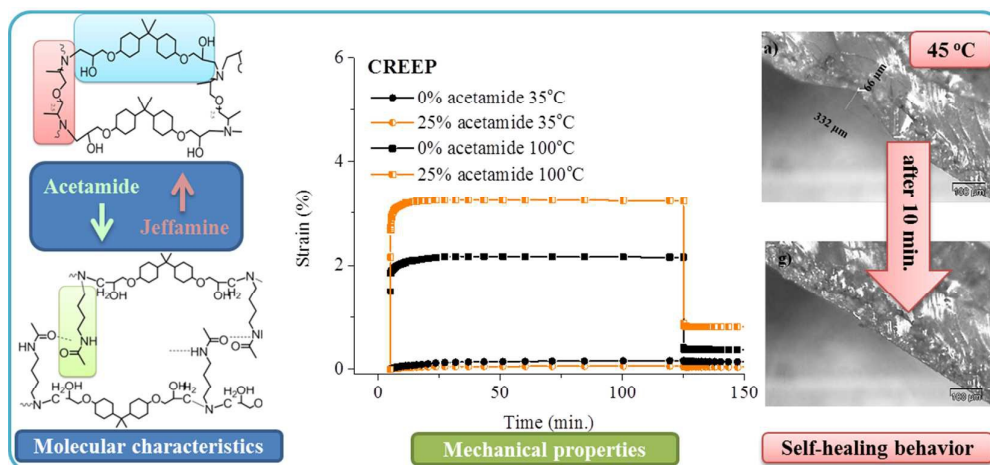
Funding Sources

This work is a part of the IOP-Self-Healing materials program in the Netherlands, from the Ministry of Economic Affairs, Agriculture and Innovation (Project No. SHM08709).

Acknowledgments

The authors thank the Dutch Ministry of Economic Affairs, Agriculture and Innovation for funding via the IOP-Self-Healing materials program (Project No. SHM08709); and Prof Rolf van Benthem (DSM Ahead, Geleen) and Ing. Leo van der Ven (AkzoNobel) for useful discussions and feedback along the research project.

Table of Contents graphic



References

1. Ghosh, S. K. Functional Coatings by Polymer Microencapsulation. In *Functional Coatings and Microencapsulation: A General Perspective*, Wiley-VCH: Weinheim, 2006.
2. Singh, H. K. Determining Interfacial Adhesion Performance and Reliability for Microelectronics Applications Using a Wedge Test Method. Virginia Polytechnic Institute and State University, Master thesis, 2004.
3. Meure, S.; Varley, R. J.; Wu, D. Y.; Mayo, S.; Nairn, K.; Furman, S. Confirmation of the Healing Mechanism in a Mendable EMAA-Epoxy Resin. *Eur Polym J* **2012**, *48* (3), 524-531.
4. Zabihi, O.; Hooshafza, A.; Moztarzadeh, F.; Payravand, H.; Afshar, A.; Alizadeh, R. Isothermal Curing Behavior and Thermo-physical Properties of Epoxy-based Thermoset Nanocomposites reinforced with Fe₂O₃ Nanoparticles. *Thermochim Acta* **2012**, *527*, 190-198.
5. Ghaffari, M.; Ehsani, M.; Khonakdar, H. A.; Van Assche, G.; Terryn, H. Evaluation of Curing Kinetic Parameters of an Epoxy/Polyaminoamide/Nano-glassflake System by Non-isothermal Differential Scanning Calorimetry. *Thermochim Acta* **2012**, *533*, 10-15.
6. Bhatnagar, M. S. Epoxy-Resins from 1980 to Date. 1. *Polym-Plast Technol* **1993**, *32* (1-2), 53-113.
7. Meis, N. N. A. H.; van der Ven, L. G. J.; van Benthem, R. A. T. M.; de With, G. Extreme Wet Adhesion of a Novel Epoxy-Amine Coating on Aluminum Alloy 2024-T3. *Prog Org Coat* **2014**, *77* (1), 176-183.
8. Hara, O., Curing Agents for Epoxy Resin. *Three Bond Technical News* 1990
9. Ramos, J. A.; Pagani, N.; Riccardi, C. C.; Borrajo, J.; Goyanes, S. N.; Mondragon, I. Cure Kinetics and Shrinkage Model for Epoxy-Amine Systems. *Polymer* **2005**, *46* (10),

- 3323-3328.
10. Ratna, D., *Handbook of Thermoset Resins*. A Smithers Group Company: 2009.
 11. Wietor, J. L.; Dimopoulos, A.; Govaert, L. E.; van Benthem, R. A. T. M.; de With, G.; Sijbesma, R. P. Preemptive Healing through Supramolecular Cross-Links. *Macromolecules* **2009**, *42* (17), 6640-6646.
 12. Tian, Q. A.; Rong, M. Z.; Zhang, M. Q.; Yuan, Y. C. Synthesis and Characterization of Epoxy with Improved Thermal Remendability based on Diels-Alder Reaction. *Polym Int* **2010**, *59* (10), 1339-1345.
 13. Canadell, J.; Goossens, H.; Klumperman, B. Self-Healing Materials based on Disulfide Links. *Macromolecules* **2011**, *44* (8), 2536-2541.
 14. Garcia, S. J., Effect of Polymer Architecture on the Intrinsic Self-healing Character of Polymers. *Eur Polym J* **2014**, *53* (1), 118-125.
 15. Gamstedt, E. K.; Talreja, R. Fatigue Damage Mechanisms in Unidirectional Carbon-fibre-reinforced Plastics. *J Mater Sci* **1999**, *34* (11), 2535-2546.
 16. Sheldon, R. P., *Composite Polymeric Materials*. Applied Science Publishers: Essex, UK, 1982.
 17. Cho, S. H.; White, S. R.; Braun, P. V. Self-Healing Polymer Coatings. *Adv Mater* **2009**, *21* (6), 645-649.
 18. Yuan, Y. C.; Yin, T.; Rong, M. Z.; Zhang, M. Q. Self Healing in Polymers and Polymer Composites. Concepts, Realization and Outlook: A review. *Express Polym Lett* **2008**, *2* (4), 238-250.
 19. Kessler, M. R.; Sottos, N. R.; White, S. R. Self-healing Structural Composite Materials. *Compos Part a-Appl S* **2003**, *34* (8), 743-753.
 20. White, S. R.; Sottos, N. R.; Geubelle, P. H.; Moore, J. S.; Kessler, M. R.; Sriram, S. R.; Brown, E. N.; Viswanathan, S. Autonomic Healing of Polymer Composites. *Nature*

- 2001**, 409 (6822), 794-797.
21. Ghosh, S. K., *Self-healing Materials: Fundamentals, Design Strategies and Applications*. Wiley-VCH Verlag GmbH&Co.: Weinheim, 2009.
 22. Dry, C. Procedures developed for Self-repair of Polymer Matrix Composite Materials. *Compos Struct* **1996**, 35 (3), 263-269.
 23. Chen, X. X.; Wudl, F.; Mal, A. K.; Shen, H. B.; Nutt, S. R. New Thermally Remendable highly Cross-linked Polymeric Materials. *Macromolecules* **2003**, 36 (6), 1802-1807.
 24. Fall, R. R. Puncture Reversal of Thylene Ionomers- Mechanistic Studies. Master thesis, Virginia Polytechnic Institute and State University, Blacksburg, Virginia, 2001.
 25. Kalista, S. J. Self-healing of Thermoplastic Poly(Ethylene-co Methacrylic Acid) Copolymers following Projectile Puncture. Master thesis, Virginia Polytechnic Institute and State University, Blacksburg, Virginia, 2003.
 26. Eisenberg, A. *Introduction to Ionomers*. John Wiley and Sons: New York, 1998.
 27. Ghosh, S. K. Studies on Elastomeric Ionomers based on EPDM Terpolymer and SEBS block copolymer. PhD thesis, Kharagpur, India, 1999.
 28. Pepels, M.; Filot, I.; Klumperman, B.; Goossens, H. Self-healing Systems based on Disulfide-thiol Exchange Reactions. *Polym Chem-Uk* **2013**, 4 (18), 4955-4965.
 29. Abdolah Zadeh, M.; Esteves, A. C. C.; van der Zwaag, S.; Garcia, S. J. Healable Dual Organic-Inorganic Crosslinked Sol-gel based Polymers: Crosslinking Density and Tetrasulfide Content Effect. *J. Polym. Sci. A Polym. Chem.* **2014**, 52 (14), 1953-1961.
 30. Zhang, B.; Digby, Z. A.; Flum, J. A.; Foster, E. M.; Sparks, J. L.; Konkolewicz, D. Self-healing, malleable and creep limiting materials using both supramolecular and reversible covalent linkages. *Polymer Chemistry* **2015**, 6(42), 7368-7372.
 31. Sordo, F.; Mougner, S. J.; Loureiro, N.; Tournilhac, F.; Michaud, V. Design of Self-

- Healing Supramolecular Rubbers with a Tunable Number of Chemical Cross-Links. *Macromolecules* **2015**, 48(13), 4394-4402.
32. Roy, N.; Buhler, E.; Lehn, J. M. Double dynamic self-healing polymers: supramolecular and covalent dynamic polymers based on the bis-iminocarbohydrazidemotif. *Polymer International* **2014**, 63(8),1400-1405.
33. Michael, P.; Döhler, D.; Binder, W. H. Improving autonomous self healing via combined chemical/physical principles. *Polymer* **2015**, 69, 216-227.
34. Döhler, D.; Peterlik, H.; Binder, W. H. A dual crosslinked self-healing system: Supramolecular and covalent network formation of four-arm star polymers. *Polymer* **2015**, 69, 264-273.
35. Bouteiller, L. Assembly via Hydrogen Bonds of Low Molar Mass Compounds into Supramolecular Polymers. *Adv Polym Sci* **2007**, 207, 79-112.
36. Dimopoulos, A.; Wietor, J. L.; Wubbenhorst, M.; Napolitano, S.; van Benthem, R. A. T. M.; de With, G.; Sijbesma, R. P. Enhanced Mechanical Relaxation below the Glass Transition Temperature in Partially Supramolecular Networks. *Macromolecules* **2010**, 43 (20), 8664-8669.
37. van Benthem, R.A.T.M.; Evers, L.J.; Mattheij, J.; Hofland, A.; Molhoek, L.J.; de Koning, A.J.; Jansen, F.G.A; van Duin, M.; Thermosets, Ch. 16 in Meyer, T.; Keurentjes, J., eds, *Handbook of Polymer Reaction Engineering*, Wiley-VCH, Weinheim, 2005.
38. Kalichevsky, M. T.; Jaroszkiewicz, E. M.; Ablett, S.; Blanshard, J. M. V.; Lillford, P. J. The Glass-Transition of Amylopectin measured by DSC, DMTA and NMR. *Carbohydr Polym* **1992**, 18 (2), 77-88.
39. Gonzalez, M. G. Applications of FTIR on Epoxy Resins - Identification, Monitoring the Curing Process, Phase Separation and Water Uptake. In *Infrared Spectroscopy -*

- Materials Science, Engineering and Technology*, Theophanides, T., Ed. Intech: 2012.
40. Nikolic, G.; Zlatkovic, S.; Cacic, M.; Cacic, S.; Lacnjevac, C.; Rajic, Z. Fast Fourier Transform IR Characterization of Epoxy GY Systems crosslinked with Aliphatic and Cycloaliphatic EH Polyamine Adducts. *Sensors-Basel* **2010**, *10* (1), 684-696.
 41. Montarnal, D.; Tournilhac, F.; Hidalgo, M.; Leibler, L. Epoxy-Based Networks combining Chemical and Supramolecular Hydrogen-Bonding Crosslinks. *J Polym Sci Pol Chem* **2010**, *48* (5), 1133-1141.
 42. Coleman, M. M.; Lee, K. H.; Skrovanek, D. J.; Painter, P. C. Hydrogen Bonding in Polymers. 4. Infrared Temperature Studies of a Simple Polyurethane. *Macromolecules* **1986**, *19*(8), 2149-2157.
 43. Miller, D. R.; Macosko, C. W. New Derivation of Post Gel Properties of Network Polymers. *Macromolecules* **1976**, *9* (2), 206-211.
 44. Lesser, A. J.; Crawford, E. The Role of Network Architecture on the Glass Transition Temperature of Epoxy Resins. *J Appl Polym Sci* **1997**, *66* (2), 387-395.
 45. Aruniit, A.; Kers, J.; Krumme, A.; Poltimae, T.; Tall, K. Preliminary Study of the Influence of Post Curing Parameters to the Particle Reinforced Composite's Mechanical and Physical Properties. *Mater Sci-Medzg* **2012**, *18* (3), 256-261.
 46. Apicella, A.; Tessieri, R.; Decataldis, C. Sorption Modes of Water in Glassy Epoxies. *J Membrane Sci* **1984**, *18* (Mar), 211-225.
 47. Urayama, K., Kawamura, T.; Kohjiya, S. Structure–mechanical property correlations of model siloxane elastomers with controlled network topology. *Polymer* **2009**, *50*(2), 347-356.
 48. de With G. *Structure, Deformation, and Integrity of Materials*. Wiley-VHC: Weinheim, 2006.

49. van Krevelen D. W.; Hoftyzer P. J. *Properties of Polymers, their Estimation and Correlation with Chemical Structure*. 2nd completely rev. ed. Amsterdam & New York: Elsevier Scientific Pub. Co., 1976.
50. Powers, D. A., *Interaction of Water with Epoxy*. Sandia Report SAND2009-4405, Albuquerque, New Mexico 2009.
51. Abdelkader, A. F.; White, J. R. Influence of Relative Humidity on the Development of Internal Stresses in Epoxy Resin based Coatings. *J Mater Sci* **2002**, *37* (22), 4769-4773.
52. Abdelkader, A. F.; White, J. R. Water Absorption in Epoxy Resins: The effects of the Crosslinking Agent and Curing Temperature. *J Appl Polym Sci* **2005**, *98* (6), 2544-2549.
53. Leibler, L. Theory of Microphase Separation in Block Co-Polymers. *Macromolecules* **1980**, *13* (6), 1602-1617.
54. Yamauchi, K.; Lizotte, J. R.; Hercules, D. M.; Vergne, M. J.; Long, T. E. Combinations of Microphase Separation and Terminal Multiple Hydrogen Bonding in Novel Macromolecules. *J Am Chem Soc* **2002**, *124* (29), 8599-8604.
55. Garcia, S. J.; Fischer, H. R.; van der Zwaag, S. A Critical Appraisal of the Potential of Self healing Polymeric Coatings. *Prog Org Coat* **2011**, *72* (3), 211-221.
56. Lafont, U.; van Zeijl, H.; van der Zwaag, S. Influence of Cross-linkers on the Cohesive and Adhesive Self-Healing Ability of Polysulfide-Based Thermosets. *Acs Appl Mater Inter* **2012**, *4* (11), 6280-6288.
57. Villani M., S. J., van Benthem R.A.T.M., de With G. Interfacial Interactions of Poly(urethane-urea) based Primers with Polypropylene. *Eur Polym J* **2014**, *56*, 118-130.